Materials Chemistry and Physics 345 (2025) 131248

Contents lists available at ScienceDirect

Materials Chemistry and Physics

journal homepage: www.elsevier.com/locate/matchemphys

Influence of bainitic transformation temperature on microstructure evolution during isothermal holding and subsequent cooling

Ehsan Tolouei [a], Mohammad Saadati [a], Jean-Benoit Morin [b], Carlos Garcia-Mateo [c], Mohammad Jahazi [a,*]

[a] Department of Mechanical Engineering, École de Technologie Supérieure ÉTS, 1100 Notre-Dame St. W, Montreal, QC, H3C 1K3, Canada
[b] Finkl Steel-Sorel, 100 McCarthy, Saint-Joseph-de-Sorel, QC, J3R 3M8, Canada
[c] Department of Physical Metallurgy, National Center for Metallurgical Research (CENIM-CSIC), Materalia Research Group, Avenida Gregorio Del Amo, 8, Madrid, 28040, Spain

HIGHLIGHTS

- Austempering temperature influences martensite formation more strongly than retained austenite content in mold steels.
- Carbon-enriched martensite from residual austenite raises local and overall hardness, as nanohardness tests confirm.
- The nanohardness method was an effective technique for comparing the local mechanical properties of different phases.

GRAPHICAL ABSTRACT

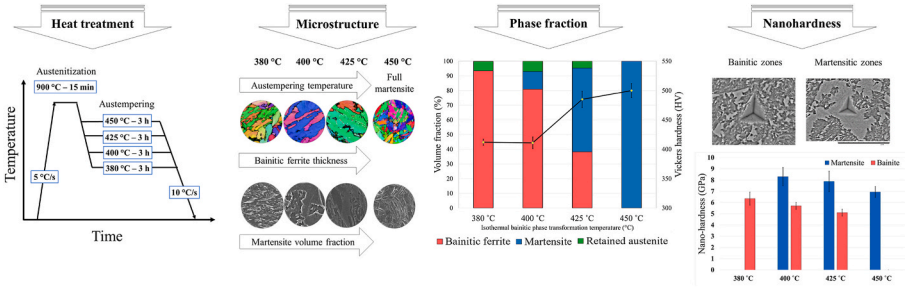

ARTICLE INFO

Keywords:
Carbon-enriched martensite
Nanohardness
Block thickness
Bainitic ferrite
Retained austenite

ABSTRACT

Modified mold steels have recently gained attention as a novel approach in steel grades due to their high-performance applications. In this study, high-resolution dilatometry was used to study the isothermal bainitic transformation of a medium-carbon low-alloy steel after full austenitization at 900 °C, followed by austempering for 3 h at temperatures ranging from 380 to 450 °C. The results showed that no bainitic phase transformation occurred at 450 °C, while an incomplete transformation was observed at all lower tested temperatures, and martensitic transformation occurred upon cooling at the final stage. Increasing the austempering temperature from 380 °C to 425 °C resulted in a lower volume fraction of bainite and a higher amount of martensite, whereas at 450 °C, a full lath martensite microstructure formed during final cooling. Electron backscatter diffraction (EBSD) and scanning electron microscopy (SEM) analyses revealed that increasing the isothermal holding temperature led to increased thickness of the bainitic blocks and a higher volume fraction of martensite. Vickers hardness increased from 412 to 500 HV between 380 and 450 °C holding temperatures. This increase was attributed to the phase volume fraction, the carbon content of martensite, and the thickness of bainitic ferrite blocks. Nanoindentation tests were conducted on different martensitic and bainitic regions to compare the influence of isothermal holding temperature on the characteristics of the phases. The results indicated that as the isothermal temperature increased, the carbon content of martensite decreased, leading to a reduction in the nanohardness of the martensitic regions from 8.3 GPa at 400 °C to 7.8 GPa at 425 °C and 6.9 GPa at 450 °C.

* Corresponding author.
E-mail address: mohammad.jahazi@etsmtl.ca (M. Jahazi).

https://doi.org/10.1016/j.matchemphys.2025.131248
Received 8 April 2025; Received in revised form 4 July 2025; Accepted 5 July 2025
Available online 7 July 2025

Furthermore, the average block thickness of bainitic ferrite increased from 0.71 μm to 1.98 μm as the isothermal temperature was raised from 380 °C to 425 °C, resulting in a decrease in nanohardness from 6.3 to 5.4 GPa. These findings are interpreted in terms of the evolution of bainitic block thickness and the carbon content of martensite at different austempering temperatures, as well as their impact on the hardness of the phases.

1. Introduction

The rapid growth of automobile and plastics production markets has significantly promoted the production of new generation of mold steels to address the ever-increasing quality requirements of the industry [1]. Specifically, microstructure uniformity and stability of mechanical properties are crucial requirements [2], particularly in the case of large size molds that have been developed in response to industry needs for very large bumpers and dashboards used in new vehicles. Medium-carbon Si-lean low-alloy steels, mostly derived from the AISI P20 family, are typically used for such applications. They are produced through ingot casting, open die forging, quenching and tempering (QT) treatments. Recently, however, in addition to conventional QT treatment, the austempering process has also been employed to heat treat these mold steels [3]. Due to the large thickness of the forged block, often more than 1000 mm, the resulting microstructure mainly consists of bainite, which offers a combination of high strength and good ductility, and has gained considerable attention in the development of modern mold steel grades [4,5].

Although bainitic microstructures offer several advantages, their complexity stems from the fact that the type, morphology, and transformation kinetics of bainite are influenced by a combination of material-related factors, such as the alloy's chemical composition [6], and process-related parameters. These include the austenitization temperature, which determines the prior austenite grain size [7], cooling rate [8], holding time and temperature in the bainitic field (commonly known as austempering) [9], etc. The mechanism of bainitic phase transformation, initiates with the nucleation and growth of bainitic ferrite (BF) plates supersaturated in carbon [10]. Upon their formation, carbon is rejected into the surrounding austenite and the subsequent plates of bainitic ferrite nucleate in a more carbon-rich austenite. As the transformation continues, the remaining austenite becomes continuously enriched in carbon, reducing the driving force for further transformation [11–13]. This process progresses until the carbon content in the remaining austenite reaches a critical point where further transformation becomes thermodynamically unfavorable. This state is described by what is known as the T_0 curve, which represents the temperature at which austenite and ferrite with the same composition possess equal free energy. This phenomenon is referred to as the 'incomplete reaction phenomenon'. The austenite that remains untransformed at this stage is termed residual austenite [10].

In the austempering process, once the isothermal bainitic phase transformation is finished the microstructure consists of BF and carbon-enriched austenite (residual austenite). During the subsequent cooling to room temperature, and depending on the carbon content of the residual austenite, it may transform into martensite, or remain stable until room temperature, resulting in what is known as retained austenite (RA) [14].

Consequently, the room temperature microstructure may be composed of BF, martensite, and RA, with multiple factors affecting the volume fraction of each phase. These variations in phase volume fractions are key drivers of changes in the mechanical properties of austempered steels.

Austempering temperature is a key factor influencing carbon supersaturation in austenite, phase fractions, transformation kinetics, and mechanical properties [15,16]. However, RA is generally undesirable in mold steels, as its transformation under stress can impair machinability and dimensional accuracy [1]. Thus, understanding RA stability during austempering is crucial for these steels. It is widely acknowledged that lowering the austempering temperature increases the volume fraction of bainite due to a higher driving force for transformation (lower free energy) [15,17,18]. As the volume fraction of bainite increases, the proportion of austenite correspondingly decreases [19]. Moreover, a higher volume fraction of bainite leads to enhanced carbon partitioning, leading to an increase in the carbon concentration within the remaining austenite [18,20]. Consequently, this carbon-enriched austenite becomes more stable, reducing the likelihood of martensite formation during the final cooling to room temperature. This stabilization allows a significant portion of the austenite to remain stable at room temperature as RA.

For instance, Lee et al. [21], studied the austempering process of a high silicon steel and found that RA initially increased with rising austempering temperature and then decreased with further temperature increase. They reported that RA stability is influenced by the $f\gamma \times C\gamma$ parameter, representing the volume fraction of RA ($f\gamma$) and its carbon content ($C\gamma$), and as the volume fraction of residual austenite increases at higher austempering temperatures, the carbon content decreases slightly, leading to reduced RA stability. In another low-carbon, high-silicon steel, Tian et al. [18], reported that decreasing the austempering temperature from 430 °C to 400 °C resulted in a 3 % increase in RA and a 20 % decrease in martensite. It is evident that the RA volume fraction and the formation of martensite during the final cooling process can be influenced by the isothermal phase transformation temperature. For example, Mondal et al. [22], reported that raising the austempering temperature by 50 °C resulted in an increase in the volume fraction of martensite from 13.5 % to 79 % in medium carbon, high-silicon steels. It is worth mentioning that other factors, such as the deformation temperature prior to austempering, and Si content influence the volume fractions of bainite and retained austenite, as reported in Refs. [23,24]. Austempering temperature affects not only phase volume fractions but also the morphology and mechanical properties of each phase. Lower temperatures refine the bainitic microstructure, while higher temperatures cause coarsening [25]. Garcia-Mateo et al. [26] highlight bainite plate thickness as key to its mechanical properties. Additionally, martensite formed at lower temperatures has higher carbon content, impacting its properties [27].

The above literature review emphasizes the importance of austempering temperature and its complex influence on determining the volume fraction of phases, the characteristics of each phase, and the resulting mechanical properties. Modifications of steel grades within the AISI P20 standard have introduced a new approach to mold steels in industrial applications. While most recent studies have focused on high-silicon steels examining, for instance, the effects of varying austempering time [28–30], and temperature [31–33] these investigations are largely limited to high-silicon compositions. Other studies have explored high-manganese steels under austempering conditions, including deformation-assisted transformations [34–36], which differ significantly from the steel grades typically used in mold applications. In high-silicon steels, silicon plays a crucial role in suppressing carbide precipitation during the bainitic transformation, leading to the formation of carbide-free bainite. As a result, the bainitic microstructures in these steels differ markedly from those in medium-carbon low-alloy steels, particularly in terms of RA volume fraction, dislocation density [37], the bainitic features size [38,39], and the volume fraction and distribution of carbides [40]. Therefore, there is a clear gap in the literature regarding the behavior of novel, modified mold steel grades under austempering conditions. From an industrial perspective, quench and temper treatments are still widely used to achieve the desired

Table 1
Chemical composition of the studied steel (wt%).

C	Mn	Si	Ni	Cr	Mo	Micro-alloys	Fe
0.26	1.15	0.35	0.70	1.50	0.55	<0.2	Balance

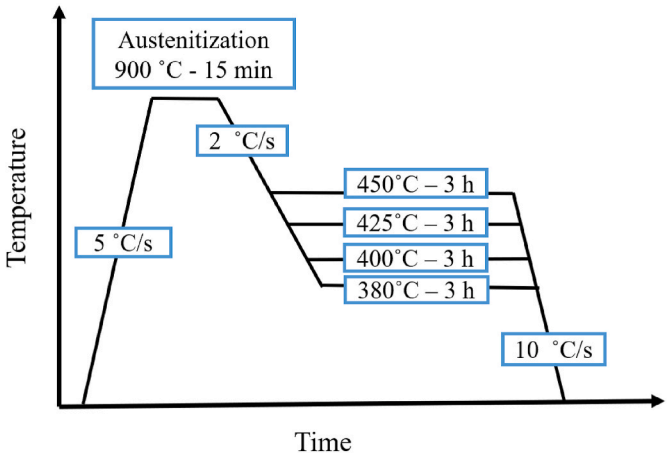

Fig. 1. Heat treatment cycle applied to the studied steel.

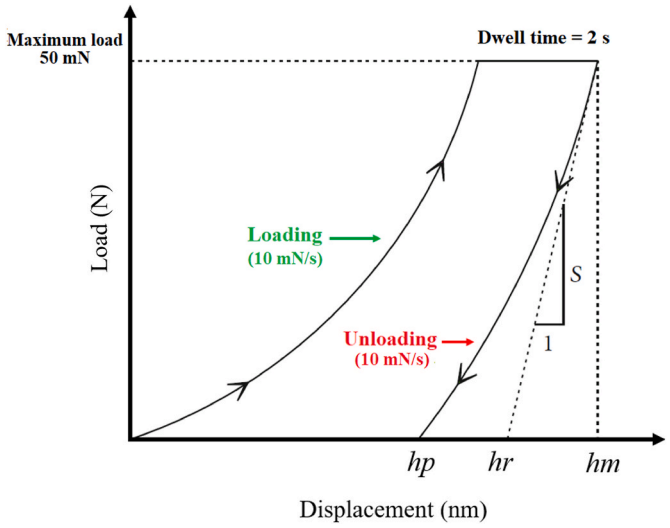

Fig. 2. Schematic of the applied nanoindentation load–displacement cycle.

mechanical properties in large forged mold steels. However, austempering presents a promising alternative that could eliminate the need for these costly and time-consuming processes. Realizing this potential requires a deeper understanding of bainitic transformation under isothermal conditions in medium-carbon low-alloy steels. Another novel aspect of the present study is the evaluation of global hardness after austempering using localized data. This was achieved through a comparative analysis of the nanohardness of individual microstructural phases, offering a new approach to characterizing bainitic microstructures.

2. Materials and methods

A medium-carbon, Si-lean low-alloy steel with the chemical composition shown in Table 1 was used in this investigation. The material, provided by Finkl Steel-Sorel, Quebec (Canada) was extracted from a large size forged and tempered block.

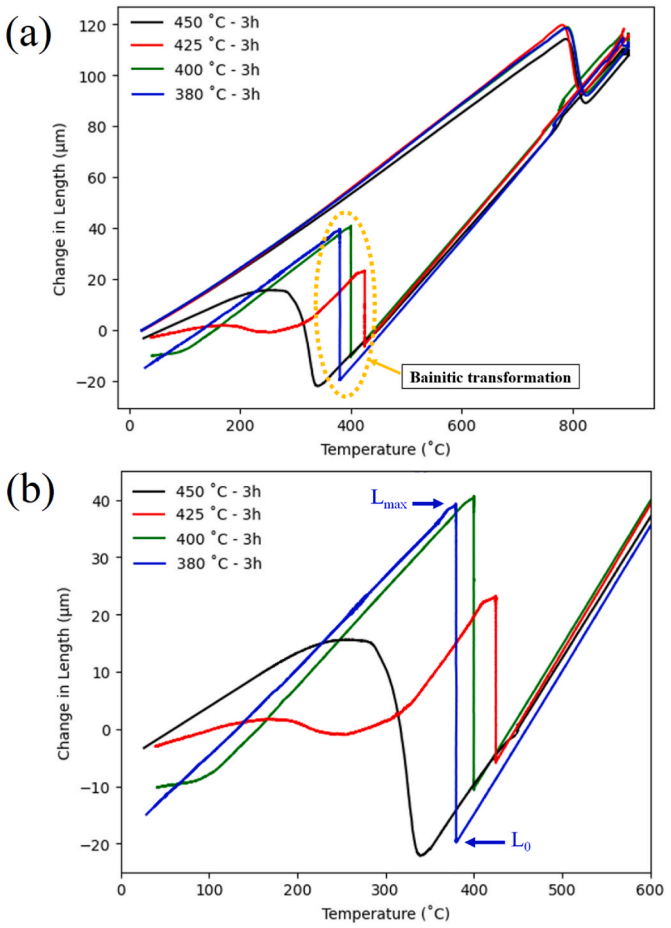

Fig. 3. Change in length as a function of temperature for the dilatometry specimens: (a) during the whole treatment as in Fig. 1; (b) magnified view of the isothermal step followed by final cooling to room temperature.

All the heat treatment experiments were conducted using a high-resolution dilatometer (Bahr 805A, TA Instruments, Hull, Germany). This instrument facilitated the detection of phase transformations during thermal cycling by monitoring the variation in length of the specimen during the whole treatment. For precise measurement of length variations, fused silica push-rods (thermal expansion coefficient; 0.54×10^{-6} °C^{-1}) were employed in conjunction with a linear variable differential transducer (LVDT), leading to a final resolution of 50 nm. The samples were heated using an induction coil, and helium gas was used for quenching. The temperature of the specimen was continuously monitored with a K-type thermocouple spot-welded to the sample surface at its mid-length. The experiments were conducted on cylindrical specimens measuring 10 mm in length and 4 mm in diameter. For the identification of austenite start and finish (Ac1 and Ac3) and martensite start and finish (Ms and Mf) transformation temperatures, the tangent method was applied to dilatometry curves. This method involves constructing tangent lines along the linear portions of the curve before and after each transformation. The points where the experimental curve deviates from these tangent lines indicate the start and finish of the transformation [41].

Fig. 1 shows the schematic of the applied heat treatment cycle. Initially, the specimens were heated at a rate of 5 °C/s to austenitization temperature at 900 °C and held for 15 min under vacuum. The samples were then cooled with a rate of 2 °C/s to different temperatures ranging from 380 °C to 450 °C, followed by 3 h holding. The selected temperatures were based on the continuous cooling transformation (CCT) diagram of the steel [42], chosen above the martensite start temperature, while the austempering time was determined based on the real

Table 2
Characteristics of samples subjected to different isothermal bainitic phase transformation treatments.

Isothermal temperature (°C)	Ms temperature (°C)	Carbon content of martensite (wt%)	Martensite volume fraction (%)	RA volume fraction (%) ±3 %	Bainitic ferrite volume fraction (%) ±3 %
450	345	0.26	100	0	0
425	328	0.29	57	4.7	38.3
400	110	1.02	12	7	81
380	<25	–	0	6.4	93.6

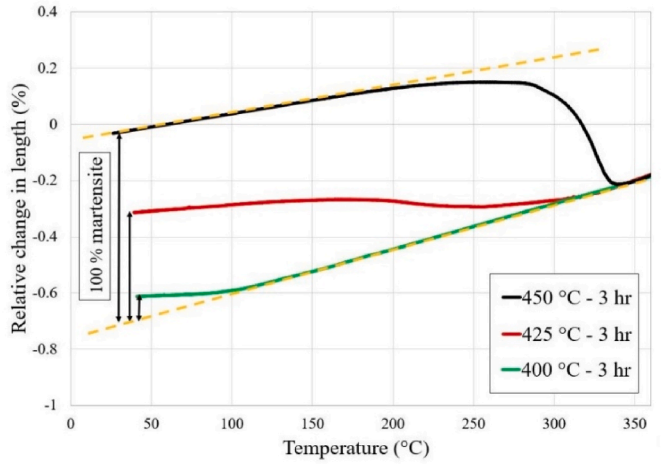

Fig. 4. Relative change in length versus temperature for the determination of martensite fraction upon cooling to room temperature.

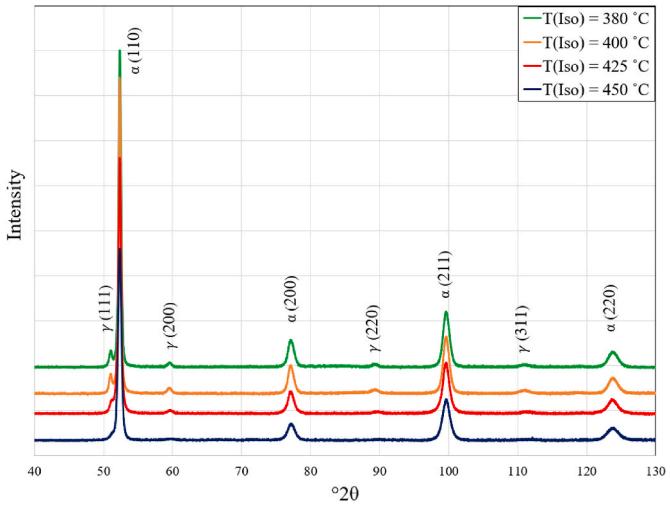

Fig. 5. XRD patterns of samples held at different austempering temperatures.

industrial scenario. In the final step, the samples were cooled to room temperature at a cooling rate of 10 °C/s.

Microstructural analysis was conducted using scanning electron microscopy (Hitachi cold field-emission SEM, Japan) after mechanical polishing and etching in 3 % Nital solution. In order to facilitate distinguishing between martensite and bainite, and for measuring the thickness of BF blocks, the electron backscatter diffraction (EBSD) technique was used. Although the EBSD phase maps do not distinguish martensite from bainite as two different phases, martensite exhibit band contrast maps of lower quality (darker) than in the case of bainite due to the higher density of lattice defects of the former as compared to the latter [43]. Bainitic block thickness was measured using EBSD data and MTEX v5.7.1 (texture and crystallography analysis toolbox) [44,45]. To accurately measure the thickness of bainitic blocks, the martensitic and bainitic regions were distinguished using band contrast EBSD images. Sample preparation for EBSD analysis involved mechanical polishing, followed by polishing with a 0.05 μm colloidal silica suspension on a Buehler VibroMet polisher, and finalizing with ion milling using an IM4000Plus system from Hitachi.

X-ray diffraction (XRD) analysis was conducted using Co Kα radiation in standard θ–2θ configuration. in order to measure the RA volume fraction. The amount of RA was determined by modified miller's method reported in ASTM E975 standard [46].

Vickers micro-hardness tests were performed using an automated tester with an applied load of 0.3 kgf and dwelling time of 10 s. On average, 10 indents were applied on the specimen's polished surface, and the reported values corresponds to an average value. Nano-indentation tests were performed at room temperature using a Hysitron PI88 SEM Picoindenter installed in a Hitachi S3600–N SEM for precise indentation positioning. A Berkovich indenter tip was used, and the equipment was calibrated with a fused silica specimen. Tests were conducted under load-control with a loading-unloading rate of 10 mN/s and a dwell time of 2 s. After initial calibration using a standard SiC reference sample, multiple trials were performed at loads ranging from 20 mN to 100 mN to evaluate result repeatability. Based on these trials, a constant load of 50 mN was selected. For reproducibility, a minimum of 5 indentations were made in each analyzed region (bainitic and martensitic). Fig. 2 illustrates a schematic representation of the load–penetration depth curve obtained from a nanoindentation experiment. The maximum displacement, denoted as *hm*, reflects the combined effect of elastic and plastic deformation. The depth where the load reduces to zero during unloading is termed the final indentation depth *hp*, representing the permanent plastic deformation. The contact stiffness S, determined at the initial stage of unloading, is calculated as the slope of the unloading curve, given by $S = dF/dh$. The parameter *hr* indicates the contact depth used to determine the contact area (*A*), which is essential for calculating the material's hardness [47]. The values for *hr* and hardness were determined using the standard Oliver and Pharr method [48]. The contact area A can be expressed as Equation (3) [49]:

$$A = 24.56h_r^2 \quad \text{Equation 3}$$

According to the Oliver and Pharr method; h_r can be calculated using to following equation [47]:

$$h_r = h_m - \varepsilon\left(\frac{F_m}{s}\right) \quad \text{Equation 4}$$

where ε is a constant which is dependent on indenter shape (ε = 0.75). The hardness is expressed as follows [49]:

$$H = \frac{P}{A} \quad \text{Equation 5}$$

3. Results and discussion

3.1. Dilatometric analysis and phase evolution

Variations in the length during the entire heat treatment cycle are shown in Fig. 3a for all tested conditions. The Ac_1 and Ac_3 temperatures

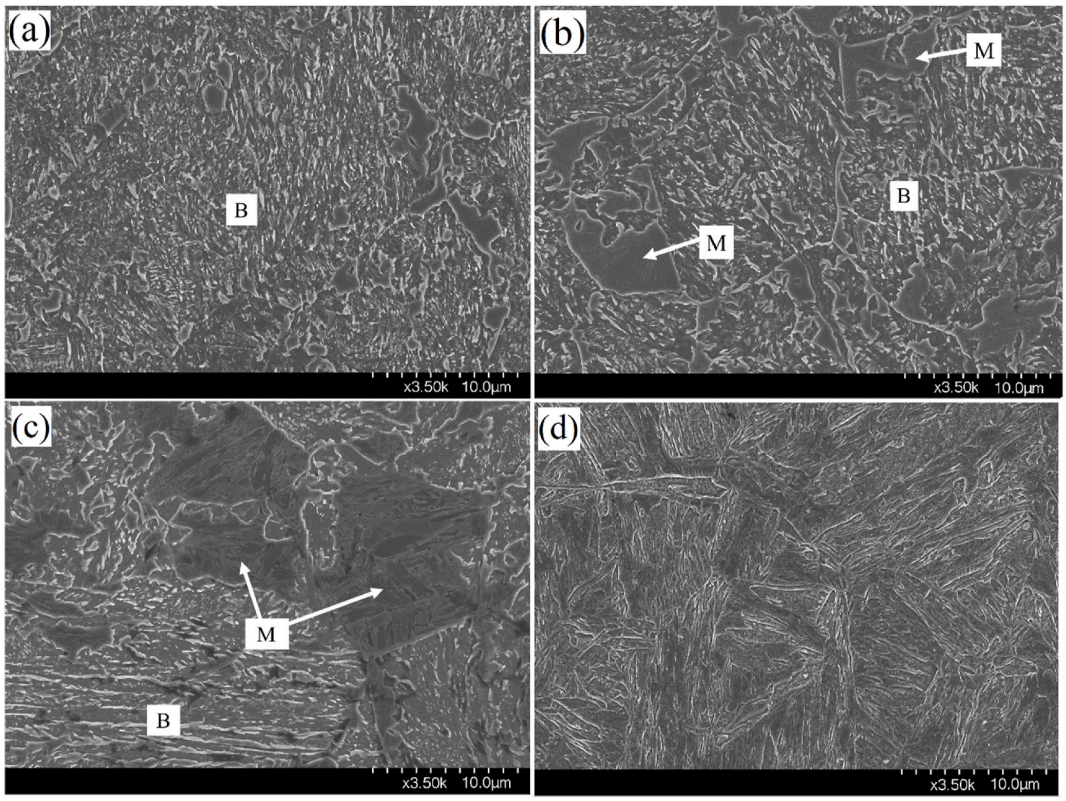

Fig. 6. SEM of the steel after different isothermal holding at (a) 380 °C, (b) 400 °C, (c) 425 °C and (d) 450 °C for 3 h. Bainite (B), retained austenite (RA), and martensite (M).

which correspond to the onset and conclusion of the austenitic transformation, were determined to be 780 °C and 825 °C, respectively, coinciding with the commencement and conclusion of the shrinkage observed during the heating process to 900 °C.

Upon cooling to the isothermal temperatures after the austenitization stage, the fully austenitic microstructure remains stable, as indicated by the linear contraction due to the decrease in temperature observed in Fig. 3, suggesting that no intermediate transformations such as ferrite/perlite occur.

Once at the targeted isothermal temperatures (Fig. 3b), and with the exception of the 450 °C treatment, an expansion of the material is observed at 380, 400 and 425 °C which is associated with the occurrence of the bainitic phase transformation [19].

As expected, the maximum length change ΔLmax (L_{max} - L_0) increases with decreasing austempering temperature (Fig. 3b) where, L_0 and L_{max} represent the sample length before and after the isothermal phase transformation. As already anticipated, this observed trend aligns with theoretical predictions and other experimental evidence [19,50], indicating that a higher fraction of BF forms at lower austempering temperatures. The greater length change is attributed to the volume expansion that occurs when austenite transforms to BF.

For the case of isothermal holding at 450 °C, as can be observed in Fig. 3b, no expansion is detected during the isothermal step, i.e. no bainitic transformation takes place. Accordingly, on cooling to room temperature, martensitic transformation of the untransformed austenite occurs, starting and finishing at 345 °C and 212 °C, respectively (Table 2).

Further analysis of the dilatometric curve of the 425 °C treatment reveals that during the final cooling stage, the martensitic transformation starts at 328 °C and finishes at 166 °C (Table 2). Similarly, for the 400 °C treatment, martensitic transformation is observed, but at the lower temperature of 110 °C (Table 2). Finally, after the formation of bainite at 380 °C, no martensitic transformation is observed.

Therefore, based on the results in Tables 2, it is clear that as the isothermal transformation temperature decreases and the amount of bainite increases, the Ms temperature also decreases, indicating an increase in the carbon content of the transformed residual austenite. Such differences in the martensite start temperature (Ms) after isothermal holdings is another notable observation, as it is not identical for all temperatures. It can be seen that lowering austempering temperature causes the Ms temperature to drop from 345 °C to below room temperature in samples held at 450 °C and 380 °C, respectively (Table 2). These changes can be explained by the nature of the bainitic transformation, in which the redistribution of carbon from supersaturated bainitic ferrite to the surrounding austenite is an inherent part of the transformation process [10]. The carbon content of the martensite formed during cooling to room temperature, after the isothermal step, can be indirectly estimated using empirical equations that relate the Ms temperature to the chemical composition of the austenite from which it forms. In the present work, the equation reported by Barbier [51] was selected, as it yield the calculated Ms value (346 °C) closest to the experimental result for the 450 °C treatment (345 °C), as shown in Table 2. Since no bainitic transformation occurred at that temperature, the carbon content of the austenite transforming to martensite corresponds to the bulk composition (Table 1). On this basis, the martensite carbon content in samples treated at the other temperatures was calculated and is summarized in Table 2. As anticipated, the results clearly show an enrichment in the residual austenite after the bainitic transformation, as the isothermal transformation temperature decreases and more bainite forms.

Dilatometric curves can be utilized to estimate the volume fraction of martensite formed during heat treatment, as described in Ref. [36] and illustrated in Fig. 4. The curve corresponding to the 450 °C treatment was used as a reference, representing a fully martensitic microstructure (100 % martensite with no RA), which was later confirmed by XRD analysis. By comparing the magnitude of length change associated with

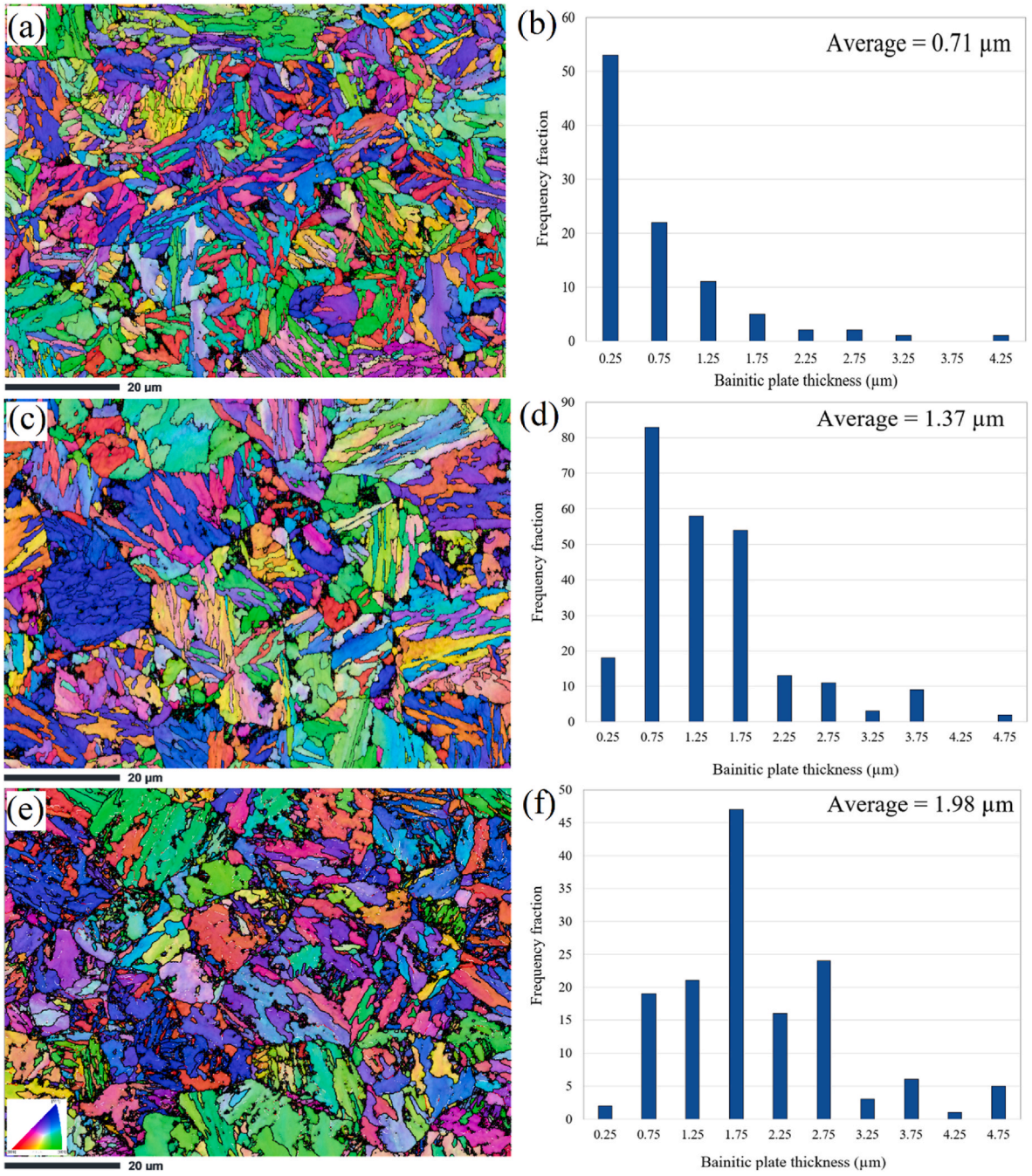

Fig. 7. EBSD map and corresponding distribution of bainitic block thickness of the steel after different isothermal holdings at, (a–b) 380 °C, (c–d) 400 °C, and (e–f) 425 °C for 3 h holding.

each isothermal holding treatment to this reference, the volume fraction of newly formed, carbon-enriched martensite was determined. For samples cooled from 400 °C and 425 °C, the estimated martensite volume fractions were 12 % and 57 %, respectively (Table 2).

3.2. Microstructure analysis

As previously stated, before the remaining residual austenite stabilizes at room temperature, a portion of it, which is low in carbon, transforms into martensite prior to reaching room temperature [52]. The volume fraction of RA at room temperature was determined using XRD and the results are reported in Table 2. For all treatments, the XRD patterns are shown in Fig. 5. It can be seen that the volume fraction of RA is close to zero at 450 °C and no γ peaks appear in the diffraction pattern. RA volume fractions increase with lowering the isothermal phase transformation temperature (380 °C and 400 °C), but none of the samples had an RA volume fraction above 10 %. The RA volume fraction was calculated to be approximately 6.4 %, 7 %, and 4.7 % at temperatures of 380 °C, 400 °C, and 425 °C, respectively. The above results are in agreement with those of Morawiec et al. [52] who observed that with decreasing austempering temperature, a higher content of stable RA with higher carbon, would be present at room temperature. Yao et al. [53] attributed this to the fact that lower austempering temperatures promote a greater degree of bainitic transformation, allowing more carbon to partition into the surrounding untransformed austenite.

Using the calculated martensite volume fraction from the dilatometry test results (Fig. 4 and Table 2) and the RA volume fraction derived from the XRD analysis, the bainite volume fraction at each temperature

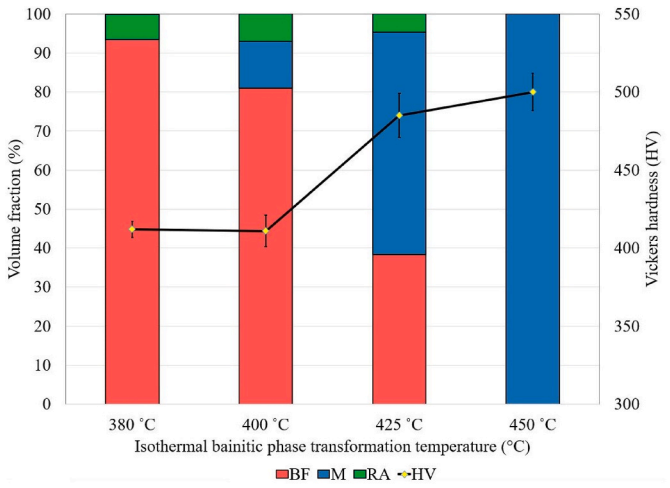

Fig. 8. Variation in micro-hardness and phase volume fraction after different isothermal treatment temperatures. Bainitic ferrite (BF), martensite (M), retained austenite (RA).

was determined as 100 - (Martensite + RA), and is summarized in Table 2. The findings indicate that as the isothermal temperature rises, the volume fraction of martensite increases, while the volume fraction of bainite decreases. This finding is in agreement with dilatometry results which showed lower expansion during bainitic phase transformation. It appears then that the lower carbon content in residual austenite at 400 and 425 °C leads to instability, causing partial transformation to martensite during final cooling.

Fig. 6 shows SEM micrographs of samples after the selected isothermal treatments. The microstructure of the samples tested at 380 °C (Fig. 6a) shows bainite and RA islands. Increasing temperature to 400 and 425 °C, Fig. 6(b and c), shows large martensite zones surrounded by bainite and dispersed RA zones. Finally, a full lath martensite microstructure can be seen in the sample tested at 450 °C (Fig. 6d). The identified microstructures are in accordance with the previous phase calculations and dilatometric experiments.

In order to measure the thickness of the BF block, the EBSD technique was employed. Fig. 7 presents the EBSD map along with the corresponding distribution of the BF thickness. The dark pixels (non-indexed regions) in the phase map represent areas where no indexing solution could be determined for the corresponding diffraction patterns either due to disproportion of selected phase parameters or could be due to lack of any patterns from the measured spot. The latter is a result of relatively high strain and a high density of lattice defects which lead to low-quality or undetectable patterns [5,43,54,55]. The martensite areas also display poor crystallographic indexing due to internal strains and dislocations, resulting in lower pattern contrast and darker regions compared to the bainitic areas, which are generally better indexed in EBSD analysis when the two phases coexist [56,57]. The bainitic block thickness was calculated using the open-source crystallographic toolbox MTEX (v5.7.1) along with MATLAB (version R2022a) add-on. In this method, it is important to note that for samples tested at 400 °C and 425 °C, where both bainite and martensite are present, measurements were performed individually for each grain. This approach ensured that martensite zones were not mistakenly identified as BF blocks. In Fig. 7 (b, d, and f), the average of the block thickness, for the sample held at 380 °C, is 0.71 μm. For the sample held at 400 °C, the average thickness range shifts to 1.37 μm and it further increases to 1.98 μm for the sample held at 425 °C. The variation in the thickness of the BF blocks cannot be attributed to a single factor; indeed, multiple factors play combined roles for the observed variations [58]. Garcia-Mateo et al. [59] reported that the thickness of the BF plates are mainly influenced by three factors: the strength of austenite at the transformation temperature, the austenite dislocation density, and the chemical free energy change associated with the transformation. However, they have reported that as the transformation temperature decreases, all the above three factors

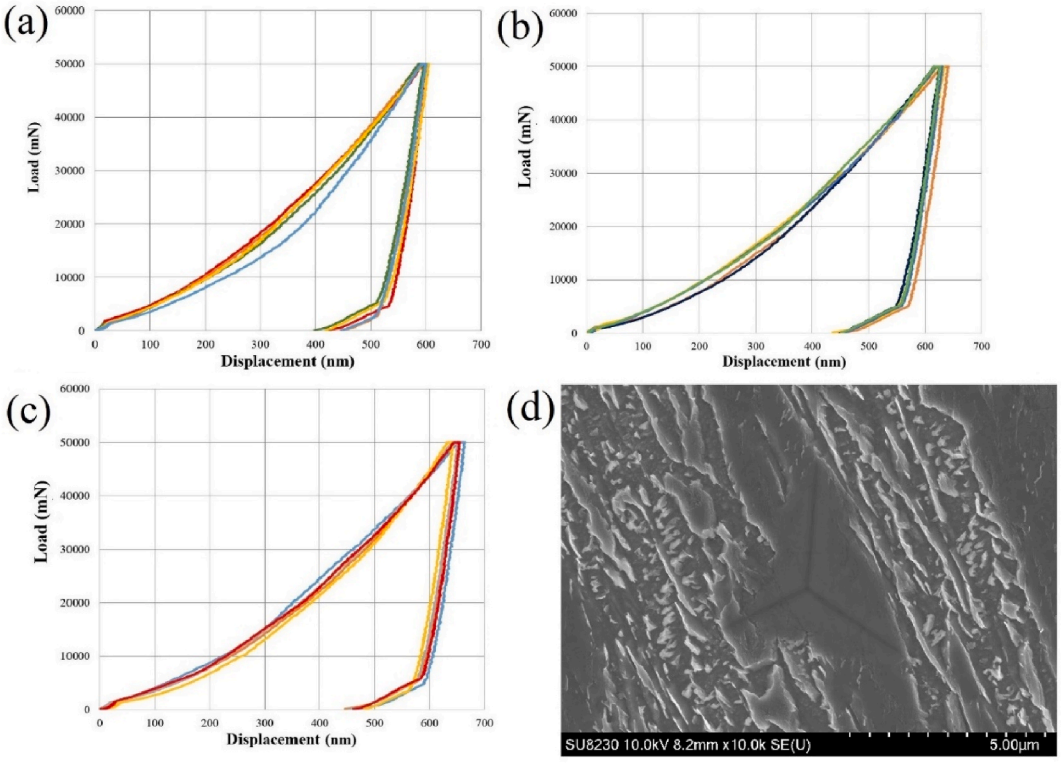

Fig. 9. Load-displacement curves obtained in a nanoindentation on the bainitic zones at different cycles (a) 380 °C, (b) 400 °C, and (c) 425 °C, and the typical SEM image after indentation on the bainitic zones (d).

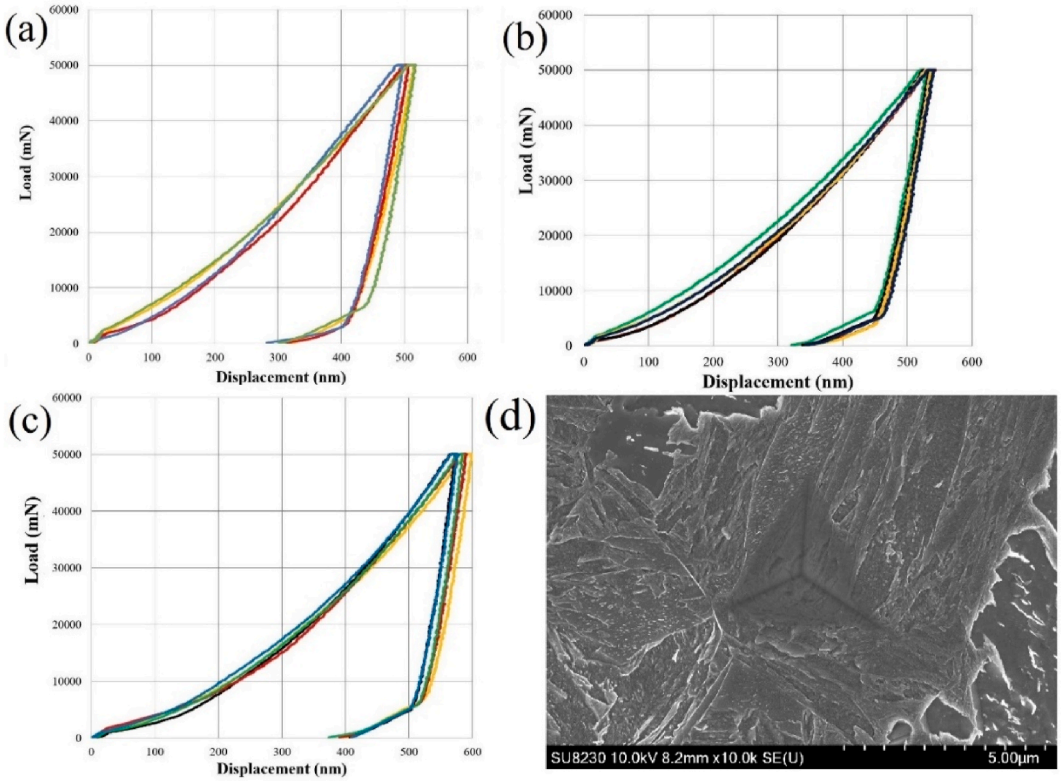

Fig. 10. Load – displacement curves obtained in a nanoindentation on the martensitic zones at different cycles (a) 400 °C, (b) 425 °C, and (c) 450 °C, and the typical SEM image after indentation on the martensitic zones (d).

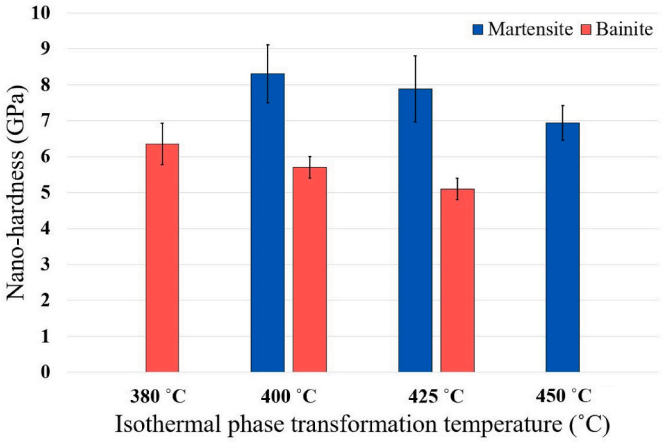

Fig. 11. Average nanohardness of bainite and martensite at different isothermal holding temperatures.

Table 3
Hardness measurement results.

Isothermal phase transformation temperature (C)	Vickers hardness (HV)	Nanohardness (bainite)	Nanohardness (martensite)
380	412 ± 5.2	6.3 ± 0.5	–
400	411 ± 9.9	5.7 ± 0.3	8.3 ± 0.8
425	485 ± 14	5.4 ± 0.2	7.8 ± 0.9
450	500 ± 12	–	6.9 ± 0.4

increase, resulting in thinner BF blocks [58].

3.3. Hardness evolution

3.3.1. Micro-hardness

Fig. 8 shows the variation in phase volume fractions and micro-Vickers hardness after different isothermal transformation temperatures. The overall trend in hardness indicates that, as the isothermal holding temperature increases, the microhardness rises. The results show that, despite different microstructures, the hardness of isothermally treated samples at 380 and 400 °C are in the same range, 412 and 411 HV, respectively. Although the amount of retained austenite is similar in both samples, the main difference between the samples held at 380 and 400 °C is the presence of 12 % martensite and bainite with thicker blocks. In bainitic microstructures, the primary factor affecting hardness is the thickness of the bainitic plates, as reported by Garcia-Mateo et al. [26]. The results indicate that while the presence of 12 % carbon-enriched martensite in the microstructure increased the variation in hardness (as evident from the error bars), the average hardness remained unchanged.

The microstructures of the samples treated at 425 °C and 450 °C exhibited significant differences (Fig. 6). At 425 °C, the microstructure comprises 38.3 % thick block bainite (1.8 μm), 4.7 % RA, and 57 % carbon-enriched martensite, resulting in a hardness of 485 HV. In contrast, the sample treated at 450 °C consists entirely of martensite with nominal carbon content, yielding a hardness of 500 HV. This comparison reveals that the lower hardness of bainite in thick block is compensated by the carbon-enriched martensite formed at lower temperatures. This observation underscores the crucial role of carbon content in determining the hardness of martensite [60].

3.3.2. Nanohardness

Despite the above reported observed differences in the carbon

content of martensite, due to the small size of martensite islands, more local analysis is needed to eliminate any interference from the neighbouring microstructural features. To this end, nanoindentation tests were performed inside the bainite and martensite zones to evaluate the mechanical properties of each of the phases at 380, 400, 425, and 450 °C.

Figs. 9 and 10 show the load-displacement curves obtained from nanoindentation tests conducted on bainite and martensite in samples treated at different temperatures, and Fig. 11 and Table 3 summaries the corresponding average nanohardness. The results clearly reveal that as the isothermal phase transformation temperature increases, the average penetration depth also increases in bainite zones. Correspondingly, as shown in Fig. 11, the average measured nanohardness decreases, with values dropping from 6.3 GPa at 380 °C to 5.7 GPa at 400 °C, and further to 5.4 GPa at 425 °C. The reduction in the thickness (1.98–0.71 μm) of the bainitic block, can be an essential factor for enhancing the hardness of austempered steels [61]. As noted earlier, the final thickness of the bainitic block is primarily influenced by several factors, and it can generally be reduced by conducting the bainitic transformation at lower temperatures [59,61,62].

Fig. 10(a–c) presents nanoindentation curves for martensite in samples treated at 400 °C, 425 °C, and 450 °C, respectively. The results reveal that the maximum depth of penetration is obtained in the martensite zones, averaging 500, 533 and 580 nm, for the samples 400, 425 and 450 °C, respectively. This observation suggests that the martensite formed at 400 and 425 °C from residual austenite with higher carbon, possesses a greater resistance to deformation in comparison to the martensite formed from primary austenite in the 450 °C sample. The average measured nanohardness was 8.3, 7.8 and 6.9 GPa for the martensite at 400, 425, and 450 °C, respectively, as reported in Fig. 11. An overview of all hardness measurements can be found in Table 3.

4. Conclusions

In this research, the influence of austempering temperature on the microstructural evolution of medium-carbon low alloy steel was investigated using high-resolution dilatometry, SEM, and EBSD. The effect of various phase fractions on overall hardness and phase-specific hardness were measured through micro-Vickers and nanoindentation methods, respectively. The following main conclusions can be drawn from this investigation:

1. The block thickness of bainitic ferrite and the carbon content of martensite significantly influence the nanohardness of these phases.
2. The refinement of the bainitic ferrite microstructure resulted from a lower austempering temperature and led to higher nanohardness.
3. Lower austempering temperatures lead to increased carbon rejection into residual austenite, resulting in the formation of martensite with higher carbon content, as confirmed by nanoindentation analysis.
4. The formation of martensite from incomplete phase transformation at higher austempering temperatures lead to greater bulk hardness compared to transformation at lower temperatures.

CRediT authorship contribution statement

Ehsan Tolouei: Writing – original draft, Methodology, Investigation, Conceptualization. **Mohammad Saadati:** Writing – review & editing, Methodology, Investigation. **Jean-Benoit Morin:** Investigation. **Carlos Garcia-Mateo:** Writing – review & editing, Supervision, Investigation. **Mohammad Jahazi:** Writing – review & editing, Validation, Supervision, Investigation.

Declaration of generative AI and AI-assisted technologies in the writing process

During the preparation of this work the authors used ChatGPT in order to only improve language and readability, with caution in some parts. After using this tool/service, the authors reviewed and edited the content as needed, and take full responsibility for the content of the publication.

Declaration of competing interest

The authors declare that they have no known competing financial interests or personal relationships that could have appeared to influence the work reported in this paper.

Data availability

The authors do not have permission to share data.

References

[1] R. Wu, et al., Improved uniformity of hardness by continuous low temperature bainitic transformation in prehardened mold steel with large section, Mater. Sci. Eng., A 706 (2017) 15–21.
[2] H. Liu, et al., Microstructure evolution and mechanical properties in 718H pre-hardened mold steel during tempering, Mater. Sci. Eng., A 709 (2018) 181–192.
[3] J. Ren, et al., Microstructure of ultrafine acicular bainite and mechanical properties of 3Cr2MnNiMo mold steel during austempering, Steel Res. Int. 93 (9) (2022) 2200151.
[4] M. Liu, et al., The effect of stress on bainite transformation, microstructure, and properties of a low-carbon bainitic steel, Steel Res. Int. 90 (10) (2019) 1900159.
[5] E. Tolouei, et al., Influence of the as quenched state and tempering temperature on the final microstructure and hardness of a high strength medium carbon steel, Mater. Chem. Phys. 325 (2024) 1–13.
[6] X.Y. Long, et al., Effect of carbon distribution range in mixed bainite/martensite/retained austenite microstructure on mechanical properties, J. Mater. Res. Technol. 17 (2022) 898–912.
[7] S. Mandal, et al., Austenite grain growth and effect of austenite grain size on bainitic transformation, Mater. Sci. Technol. 38 (7) (2022) 409–418.
[8] Y. Zhang, et al., Effect of ultra-fine martensite and retained austenite induced by slow quenching on the mechanical properties of 9Cr 1.5Mo1Co(FB2) steel, Mater. Char. 181 (2021) 111452.
[9] C. Liu, et al., Acicular ferrite formation during isothermal holding in HSLA steel, J. Mater. Sci. 51 (2016) 3555–3563.
[10] H.K.D.H. Bhadeshia, Bainite in Steels: Transformations, Microstructure and Properties, second ed., IOM Communications, 2001.
[11] Elena Pereloma, D.V. Edmonds, Phase Transformations in Steels, vol. 2, Woodhead Publishing Limited, 2012.
[12] J. Zhao, et al., Effects of austempering temperature on bainitic microstructure and mechanical properties of a high-C high-Si steel, Mater. Sci. Eng., A 742 (2019) 179–189.
[13] H. Bhadeshia, A. Waugh, Bainite: an atom-probe study of the incomplete reaction phenomenon, Acta Metall. 30 (4) (1982) 775–784.
[14] C. Garcia-Mateo, et al., On measurement of carbon content in retained austenite in a nanostructured bainitic steel, J. Mater. Sci. 47 (2) (2012) 1004–1010.
[15] X.Y. Long, et al., Effect of austempering temperature on microstructure and cyclic deformation behaviour of multiphase low-carbon steel, Arch. Civ. Mech. Eng. 23 (3) (2023) 201.
[16] Y. Su, et al., Effect of austempering temperature on microstructure and mechanical properties of M50 bearing steel, J. Mater. Res. Technol. 20 (2022) 4576–4584.
[17] H.K.D.H. Bhadeshia, J.W. Christian, Bainite in steels, Metall. Trans. A 21 (3) (1990) 767–797.
[18] J. Tian, et al., Refined bainite microstructure and mechanical properties of a high-strength low-carbon bainitic steel treated by austempering below and above MS, Steel Res. Int. 89 (4) (2018) 1700469.
[19] B. Gao, et al., Accelerated isothermal phase transformation and enhanced mechanical properties of railway wheel steel: the significant role of pre-existing bainite, Steel Res. Int. 93 (2) (2022) 2100494.
[20] M. Franceschi, et al., Effect of different austempering heat treatments on corrosion properties of high silicon steel, Mater 14 (2) (2021) 288.
[21] Y.K. Lee, et al., Effect of isothermal transformation temperature on amount of retained austenite and its thermal stability in a bainitic Fe–3%Si–0.45%C–X steel, Scr. Mater. 47 (12) (2002) 805–809.
[22] J. Mondal, K. Das, S. Das, Isothermal transformation kinetics, microstructure and mechanical properties of a carbide free bainitic steel, Mater. Char. 177 (2021) 111166.
[23] M. Franceschi, et al., Effect of ausforming temperature on bainite morphology in a 3.2% Si carbide-free bainitic steel, Mater. Sci. Eng., A 864 (2023) 144553.
[24] H.K.D.H. Bhadeshia, D.V. Edmonds, The bainite transformation in a silicon steel, Metall. Trans. A 10 (1979) 895–907.
[25] Y. Han, et al., Microstructures and mechanical characteristics of a medium carbon super-bainitic steel after isothermal transformation, J. Mater. Eng. Perform. 23 (12) (2014) 4230–4236.
[26] C. Garcia-Mateo, F.G. Caballero, H.K.D.H. Bhadeshia, Development of hard bainite, ISIJ Int. 43 (8) (2003) 1238–1243.

[27] X. Wang, et al., Enhancing strength-ductility combination in a novel Cu–Ni bearing Q&P steel by tailoring the characteristics of fresh martensite, J. Mater. Res. Technol. 24 (2023) 9015–9029.
[28] Q. Luo, et al., Effect of short-term low-temperature austempering on the microstructure and abrasive wear of medium-carbon low-alloy steel, Met. Mater. Int. 27 (9) (2021) 3115–3131.
[29] D. Bhuyan, et al., Effect of austempering time on bainite plate thickness and variant selection in a high carbon low alloy steel, Mater. Char. 200 (2023) 112923.
[30] Y. Han, et al., Isothermal transformation of a commercial super-bainitic steel: part I microstructural characterization and hardness, J. Mater. Eng. Perform. 26 (2) (2017) 472–477.
[31] S.H. Kim, et al., Microstructure and mechanical properties of austempered medium-carbon spring steel, Met. Mater. Int. 24 (4) (2018) 693–701.
[32] S.K. Putatunda, C. Martis, J. Boileau, Influence of austempering temperature on the mechanical properties of a low carbon low alloy steel, Mater. Sci. Eng., A 528 (15) (2011) 5053–5059.
[33] S. Pashangeh, et al., On the decomposition of austenite in a high-silicon medium-carbon steel during quenching and isothermal holding above and below the Ms temperature, Mater. Char. 162 (2020) 110224.
[34] A. Grajcar, P. Skrzypczyk, A. Kozłowska, Effects of temperature and time of isothermal holding on retained austenite stability in Medium-Mn steels, Appl. Sci. 8 (11) (2018) 2156.
[35] A. Grajcar, H. Krztoń, Effect of isothermal holding temperature on retained austenite fraction in medium-carbon Nb/ti-Microalloyed TRIP steel, J. Achiev. Mater. Manuf. Eng. 49 (2011) 391–399.
[36] M. Morawiec, et al., Study of the isothermal bainitic transformation and austenite stability in an advanced Al-rich medium-Mn steel, Arch. Civ. Mech. Eng. 22 (4) (2022) 152.
[37] X.Y. Long, et al., Study on carbide-bearing and carbide-free bainitic steels and their wear resistance, Mater. Sci. Technol. 33 (5) (2017) 615–622.
[38] R. Branco, et al., Comparative study of the uniaxial cyclic behaviour of carbide-bearing and carbide-free bainitic steels, Metals 8 (6) (2018) 422.
[39] X. Long, et al., Study on microstructures and properties of carbide-free and carbide-bearing bainitic steels, Mater. Sci. Eng., A 715 (2018) 10–16.
[40] O. Gulbay, et al., Influence of transformation temperature on the high-cycle fatigue performance of carbide-bearing and carbide-free bainite, Steel Res. Int. 94 (12) (2023) 2300238.
[41] J. Uchil, K.K. Mahesh, K. Ganesh Kumara, Dilatometric study of martensitic transformation in NiTiCu and NiTi shape memory alloys, J. Mater. Sci. 36 (24) (2001) 5823–5827.
[42] V. Hurel, Optimazation of the Heat Treatment of a Steel with High Mechanical Resistance, Ecole de technology superior, 2022, p. 60. Mechanic department. Master thesis.
[43] M.-S. Baek, et al., Quantitative phase analysis of martensite-bainite steel using EBSD and its microstructure, tensile and high-cycle fatigue behaviors, Mater. Sci. Eng., A 785 (2020) 139375.
[44] F. Bachmann, R. Hielscher, H. Schaeben, Texture analysis with MTEX – free and open source software toolbox, Solid State Phenom. 160 (2010) 63–68.
[45] The MathWorks, I. R2022a. https://www.mathworks.com, 2022.
[46] A. Committee, Standard Practice for X-Ray Determination of Retained Austenite in Steel with near Random Crystallographic Orientation, 100 Barr Harbor Drive, PO Box C700, ASTM International, 2013, p. 7.
[47] Y. Mazaheri, A. Kermanpur, A. Najafizadeh, Nanoindentation study of ferrite–martensite dual phase steels developed by a new thermomechanical processing, Mater. Sci. Eng., A 639 (2015) 8–14.
[48] W.C. Oliver, G.M. Pharr, An improved technique for determining hardness and elastic modulus using load and displacement sensing indentation experiments, J. Mater. Res. 7 (6) (1992) 1564–1583.
[49] M. Lei, et al., Study on the effect of nanoindentation test method on micromechanical properties of granite minerals, Geofluids (2022).
[50] C. Rampelberg, et al., Carbide-free bainite transformations above and below martensite start temperature investigated by In-Situ high-energy X-Ray diffraction, J. Occup. Med. 73 (11) (2021) 3181–3194.
[51] D. Barbier, Extension of the martensite transformation temperature relation to larger alloying elements and contents, Adv. Eng. Mater. 16 (1) (2014) 122–127.
[52] M. Morawiec, et al., Thermodynamic analysis and isothermal bainitic transformation kinetics in lean medium-Mn steels, J. Therm. Anal. Calorim. 142 (5) (2020) 1709–1719.
[53] C. Yao, et al., Enhanced strength and toughness of low-carbon bainitic steel by refining prior austenite grains and austempering below Ms, Steel Res. Int. 92 (11) (2021) 2100263.
[54] B.-Y. Jeong, R. Gauvin, S. Yue, EBSD study of martensite in a dual phase steel, Microsc. Microanal. 8 (S02) (2002) 700–701.
[55] N. Isasti, et al., Analysis of complex steel microstructures by high-resolution EBSD, J. Occup. Med. 68 (1) (2016) 215–223.
[56] S. Pashangeh, et al., Detection and estimation of retained austenite in a high strength Si-Bearing bainite-martensite-retained austenite micro-composite steel after quenching and bainitic holding (Q& B), Metals 9 (5) (2019) 492.
[57] A. Navarro-López, et al., Characterization of bainitic/martensitic structures formed in isothermal treatments below the Ms temperature, Mater. Char. 128 (2017) 248–256.
[58] J. Cornide, et al., An assessment of the contributing factors to the nanoscale structural refinement of advanced bainitic steels, J. Alloys Compd. 577 (2013) S43–S47.
[59] C. Garcia-Mateo, et al., Transferring nanoscale bainite concept to lower C contents: a perspective, Metals 7 (2017), https://doi.org/10.3390/met7050159.
[60] K. Kwak, et al., Correlation between strength and hardness for substructures of lath martensite in low- and medium-carbon steels, Mater. Sci. Eng., A 856 (2022) 144007.
[61] A. Skowronek, et al., Bainite plate thickness reduction and microstructure tailoring by double austempering of Al-rich 3Mn steel, Mater. Sci. Eng., A 853 (2022) 143743.
[62] Y. Huang, et al., Microstructure, crystallography and nucleation mechanism of NANOBAIN steel, Int. J. Miner. Metall. Mater. 20 (12) (2013) 1155–1163.